J Mater Sci: Mater Electron (2012) 23:1830–1834
DOI 10.1007/s10854-012-0670-4

The formation of quantum dot structures in 30-pair InGaN/GaN multiple quantum wells after proper thermal annealing treatment

Yen-Sheng Lin · Ho-Hung Kuo · Shih-Wei Feng

Received: 14 January 2012 / Accepted: 21 February 2012 / Published online: 1 March 2012
© Springer Science+Business Media, LLC 2012

Abstract This study systematically investigates the relation between strain energy and quantum dot (QD) formation for 30- pair InGaN/GaN multiple quantum wells (QW) by means of atomic force microscopy and high-resolution transmission electron microscopy. The results show that a higher number of quantum wells induce a higher strain energy and higher density of V-shaped defects, which increases the number of non-radiative centers. However, after thermal annealing, the strain energy accumulated from stacking faults is released and leads to the formation of a QDs structure. The strain energy around the quantum dot structure was calculated using by the NCEM Phase Extensions to the Digital Micrograph. The zone of higher strain energy was observed, which proves that the strain energy is the driving force for the formation of quantum dot structures.

1 Introduction

V-shaped and quantum dot-like structures are commonly observed in InGaN/GaN quantum wells (QW). Such “defects” are formed because of the large lattice mismatch, about 11%, between the InGaN and GaN layers. One of the major problems caused by V-shaped defects is the potential fluctuation that is associated with carrier localization [1–3]. The mechanism of carrier localization has been widely used to interpret the observed optical characteristics of these compounds and to explain the S-shape in the temperature dependence of the photoluminescence (PL) peak [4, 5]. The large lattice mismatch between InGaN wells and GaN barriers leads to a accumulation of strain at the layer boundaries, causing a strain-induced piezoelectric field that provokes the quantum-confined Stark Effect (QCSE), which in turn provides an explanation for measured optical phenomena such as the excitation power dependence of the PL spectral peak [6–8]. QCSE causes spatially separated electron and hole wave functions, a reduced radiative transition rate and a longer PL decay time [9, 10]. It is widely believed that the effects of both carrier localization and the quantum-confined Stark Effect (QCSE) play specific roles in the photon emission mechanisms in such compound structures. Ho et al. [11] found that the size, shape, composition, and distribution of the indium-aggregated clusters depended on the nominal indium content in InGaN and the degree of spinodal decomposition. Randomly distributed clusters of indium aggregation and phase-separated InN have frequently been observed by means of HRTEM. The cluster structures form potential minima (localized states) that trap carriers for efficient photon emission [5, 12–14]. Since strain energy is unavoidably induced during the growth of the InGaN QW layers, an investigation of the effect of cluster formation on photon emission characteristics requires the use of growth methods for different growth pairs and annealing conditions [15, 16]. Bimberg et al. [17] and Hsu et al. [18] reported that for the indium arsenide system, post-growth thermal annealing can alter the size and distribution of self-organized quantum dots. A similar influence of

Y.-S. Lin (✉)
Department of Electronic Engineering, I-Shou University, Kaohsiung, Taiwan, ROC
e-mail: yslin@isu.edu.tw

H.-H. Kuo
Department of Production Systems Engineering, Toyohashi University of Technology, Toyohashi, Japan

S.-W. Feng
Department of Applied Physics, National University of Kaohsiung, Kaohsiung, Taiwan, ROC

post-growth thermal annealing on the cluster structure and photon emission properties has also been noted for InGaN [19–21]. As reported in a recent study [21], such influence can be reduced by compositional non-homogeneity at an early stage of thermal annealing. Using this approach, better-confined quantum well structures with less indium out-diffusion and increasing PL were obtained [21]. This was also confirmed in a later study, which proved that the formation of regularly embedded InGaN or InN quantum dots (QDs) around the well layers and appropriate post thermal treatment can significantly increase the PL intensity [22]. This shows that optimum post-growth thermal treatment is a crucial process parameter for the fine- tuning of the photon emission, wavelength, and spectral gain of InGaN compounds.

2 Experimental

All specimens were prepared by depositing InGaN/GaN multiple quantum wells (MQWs) on c-plane sapphire substrates using metal organic chemical vapor deposition (MOCVD) [23]. Following the deposition of a 1.5 µm GaN buffer layer and then a 23 nm GaN barrier layer, the MQW structure was fabricated by depositing stacks of one to 30 pairs of $In_{0.15}Ga_{0.85}N$/GaN bi-layers. The deposition temperatures for the GaN and InGaN layers were 1,010° and 720 °C, respectively. The annealed specimens were prepared by annealing the as-deposited specimens for 10–30 min in a nitrogen atmosphere in a quartz tube furnace, at temperatures from 800 °C to 900 °C. X-ray diffraction measurements were performed using a standard diffractometer with monochromated Cu-K α radiation. The composition of $In_xGa_{1-x}N$ was determined from the lattice spacing of the 0002 Bragg peak, using Vegard's law [24]. The density of pitting defects and surface morphologies was examined by atomic force microscopy (AFM), performed in the tapping mode. Cross-sectional samples were prepared by the conventional sandwich technique [25]. A cross-sectional sample was prepared in a conventional manner by grinding, dimpling and Ar^+-ion milling, at 6 kV, 1 mA and an incident angle of 4°. However due to previous experience with In coating materials, the ion milling step was always performed with the specimen holder at the temperature of liquid nitrogen, in order to minimize the ion beam damage. The HRTEM investigations were performed in both 200 keV Philips CM 200 and 300 keV JEM 3010 microscopes. All high-resolution micrographs were taken at Scherzer defocus and the sample was viewed along a $[11\bar{2}0]$ zone axis, using a 300 keV JEM 3010 microscope equipped with a 2 k × 2 k slow-scan CCD camera and a Gatan Imaging Filter (GIF) [26]. The strain energy distribution was calculated using the NCEM Phase Extensions to the Digital micrograph [27]. For time-resolved photoluminescence (TRPL) measurements, a picosecond diode laser (PicoQuant) generated optical pulses of 100 ps width with a 5 MHz repetition rate to excite the epilayers [28].

3 Results and discussion

The AFM images of as-grown (a) 1-, (b) 5-, (c) 10- and (d) 30-pair $In_{0.15}Ga_{0.85}N$/GaN MQWs specimens are shown in Fig. 1. A higher defect density was observed for 30-pair samples. Most of the defects joined with nearby defects, since the higher strain energy is released through the formation of thread dislocations or local lattice distortions in the QW layers, which also lead to quite poor photon emission efficiency. The TEM images along the $[11\bar{2}0]$ zone axis of the cross-section of the as-grown 10-pair and 30-pair specimens are shown in Figs. 2 and 3, respectively. The formation of V-shaped defects of edge and screw type was observed. In Fig. 2a, the smaller V-shaped defects are shown the magnified view of the area enclosed by the white rectangle in Fig. 2a is shown in Fig. 2b. The threading dislocation obviously extends into a number of QW pairs and terminates at the V-shaped defect. The size of the V-shaped defects increases with the number of QW pairs, due to the larger strain energy. This suggests that the threading dislocation continuously grows by the coalescence of misfit dislocations in every QW pair, as shown in

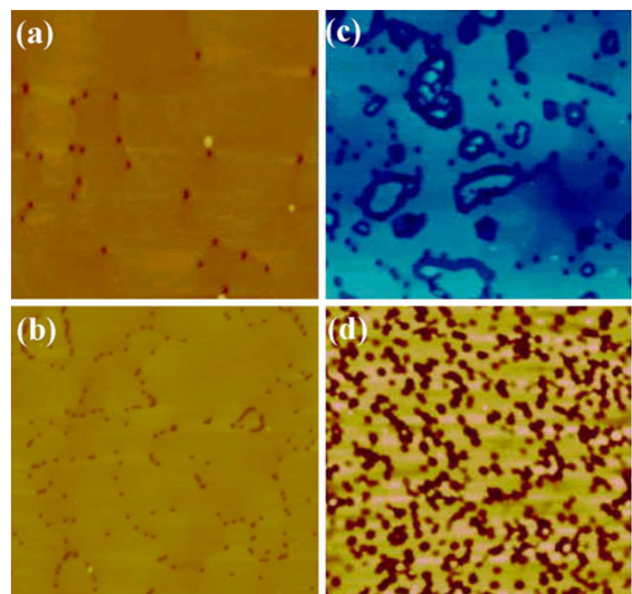

Fig. 1 AFM surface images of as-grown (**a**) 1-, (**b**) 5-, (**c**) 10- and (**d**) 30-pair $In_{0.15}Ga_{0.85}N$/GaN QW specimens, obtained from a 2 µm × 2 µm square

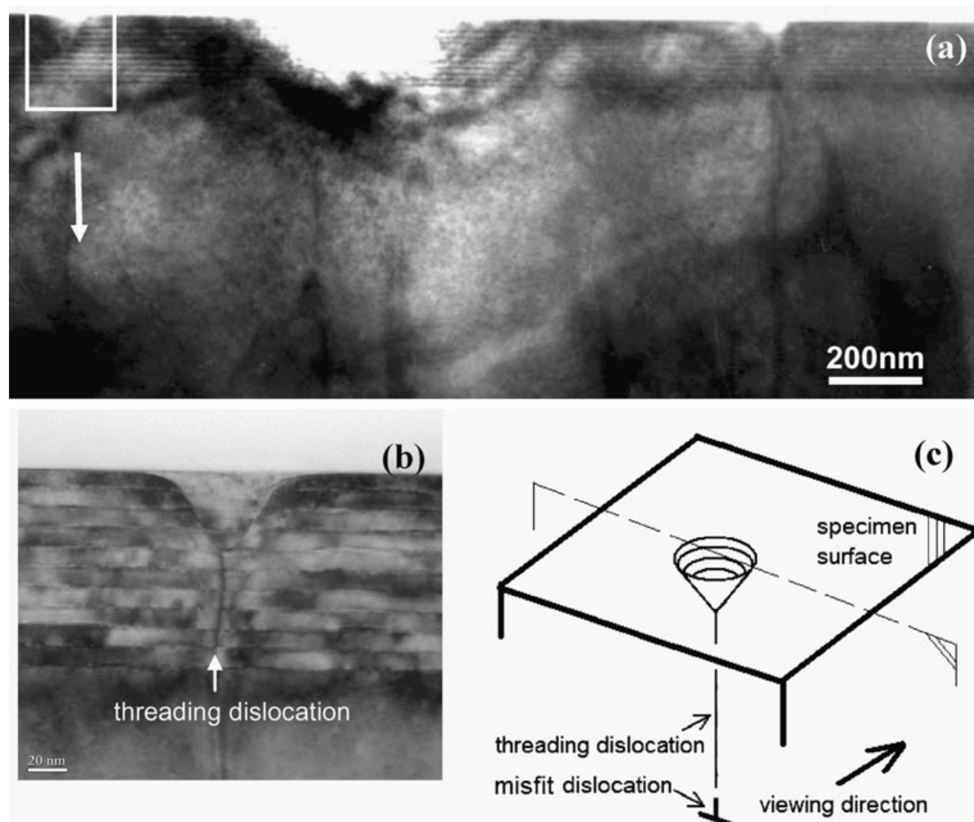

Fig. 2 TEM images of a conventionally prepared cross-sectional sample- (**a**) V-shaped defects in the as-grown 10-pair specimen, (**b**) magnified view of the V-shaped defect from the area enclosed by the white rectangle in (**a**); (**c**) a *schematic diagram* showing a V-shaped defect

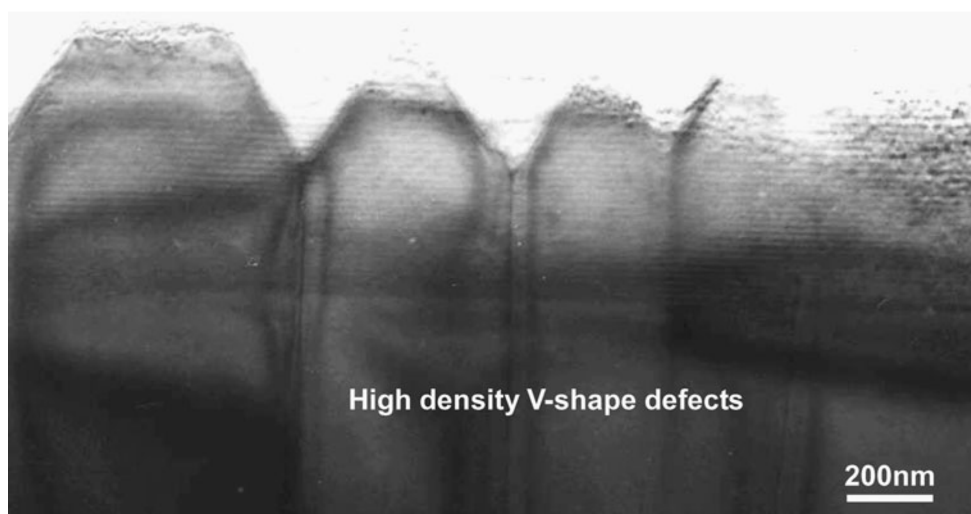

Fig. 3 A cross-sectional TEM *bright-field image* showing the pitting defects in the as-grown 30-pair specimen

Fig. 3, until the point at which the formation of further misfit dislocations is no longer capable of compensating for the strain energy caused by the growth of QWs. Hence, the density of the V-shaped defects increases as the number of QW pairs increases. Analysis of the AFM top-view and the TEM side-view images indicates that V-shaped defects are essentially misfit dislocations triggered by the lattice misfit between the InGaN and GaN layers. The V-shaped defects are gradually formed from mixed type, which includes edge and screw type. Figure 3 shows that the observed starting point of the opening of the V-shape core is different, due to the different strain energy released during the growth process. Compared to the 10-pair specimen, the 30-pair specimen contains a much higher density of defects. As a result, the microstructural evolution of the increasing the number of MQW's causes the formation of

defect clusters, as verified by AFM examination, and thus provides a reasonable explanation for the unusually poor photon emission efficiency. Therefore, decreasing the number of V-shaped defects by optimizing the thermal annealing process appears to be the most promising method. Figure 4 shows the HRTEM images of the 30-pair specimen for various thermal annealing treatments. During initial thermal annealing, an irregular atomic arrangement is observed, as shown in Fig. 4a. Most of this occurs due to misfit dislocations. The stacking faults and QDs structures are observed in Fig. 4c, which suggests that the strain energy is the driving force for the formation of QDs. The strain energy in these areas is released through the creation of partial dislocations and stacking faults. This implies that the interfacial strain caused by the lattice misfit is necessarily almost entirely localized at the QD after thermal annealing. The formation of QD leads to potential fluctuations and causes carrier localization. In order to prove the existence of a higher strain energy around the quantum dot structure, the NCEM Phase Extensions to Digital Micrograph were used to calculate the distribution of strain energy, as shown in Fig. 5 [27]. The higher strain energy zone is indicated by a white arrow. This result shows that the defect structures and indium segregation accommodate the strain energy of incoherence or semi-coherence between the lattices of InGaN and GaN [29]. During the thermal annealing process, the misfit dislocations act like energy sinks that force diffused indium atoms to approach them. Because of the increase in the strain energy caused by the diffusion of indium into the lattice, new misfit dislocations are generated and these begin to form partial dislocations and subsequently develop into stacking faults, in order to release the excess strain energy. Consequently, Indium-rich quantum dot structures become highly

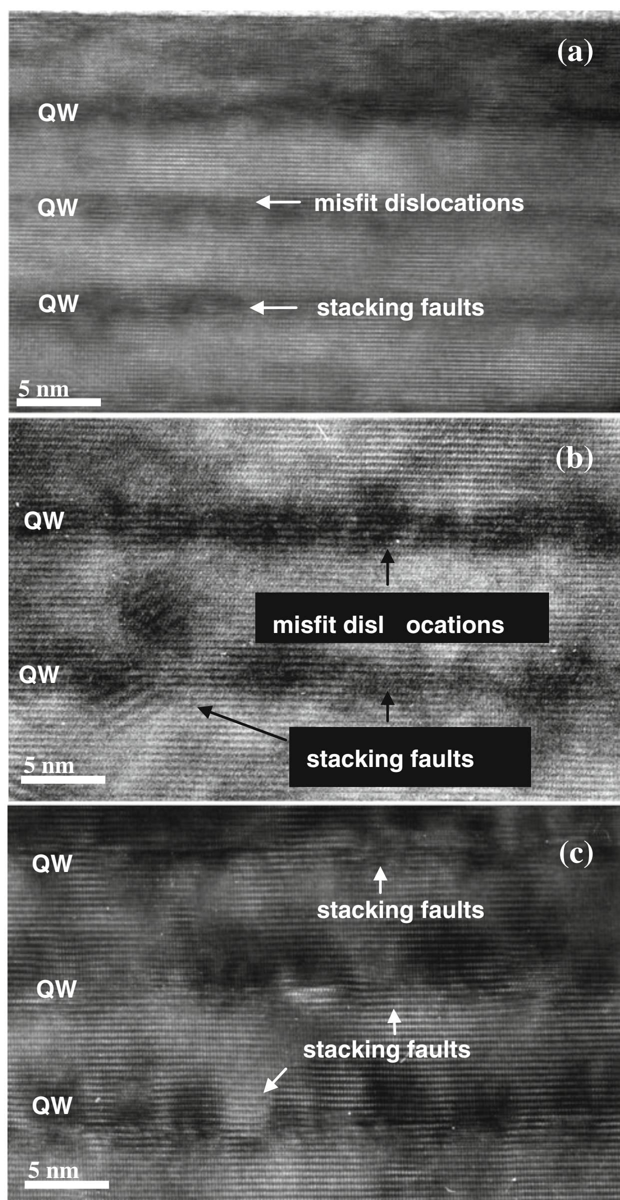

Fig. 4 HRTEM images of the 30-pair specimen with 800 °C thermal annealing treatment for (**a**) 10 (**b**) 20 and (**c**) 30 min-, the *arrows* indicate the difference between stacking faults and misfit dislocations

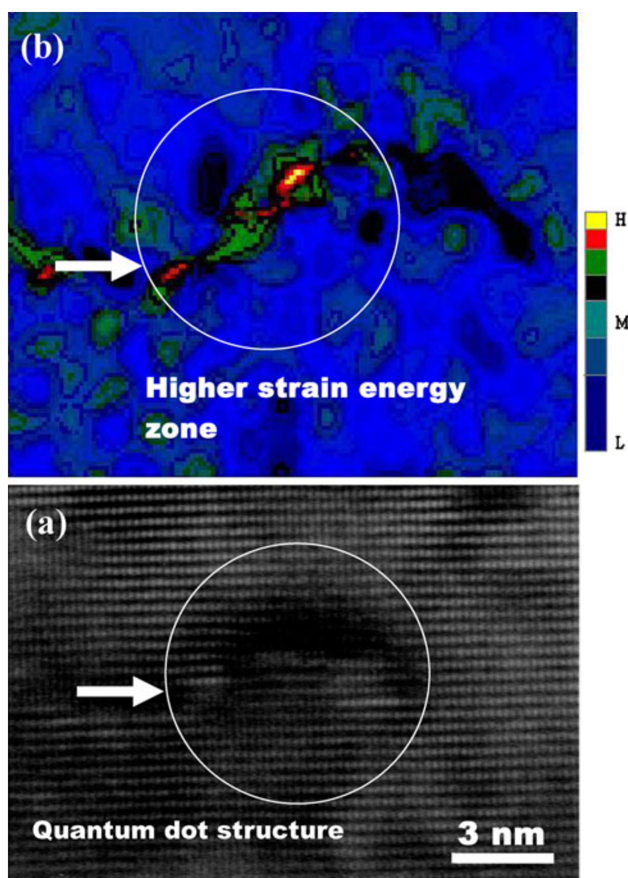

Fig. 5 (**a**) An atomic-scale HRTEM image of the quantum dot structure and (**b**) the calculation of the strain energy by NCEM Phase Extensions to the Digital Micrograph

localized at the InGaN/GaN interface and lead to a localisation of the higher strain-field zone around the QDs.

4 Conclusion

The effect of microstructural evaluation on the material of 1–30-pair InGaN/GaN MQWs was investigated. It is observed that the density of V-shaped defects depends strongly on the number of quantum wells, due to the larger strain energy comes from threading dislocations. After 800 °C thermal annealing treatment for 30 min, the more obvious quantum dot structures were formed in 30-pair InGaN/GaN MQWs, and the higher strain-field zone around the QDs was also calculated, which means the strain energy play an important role as driving force for the formation of quantum dot structures.

Acknowledgments This research was supported by the National Science Council, Republic of China, under grants NSC 96-2623-7-214-002-NU and NSC96-2221-E-214-019-MY2.

References

1. Y. Narukawa, Y. Kawakami, M. funato, S. Fujita, S. Kawakami, Appl. Phys. Lett. **70**, 981 (1997)
2. M.D. McCluskey, L.T. Romano, B.S. Krusor, D.P. Bour, N.M. Johnson, S. Brennan, Appl. Phys. Lett. **72**, 1730 (1998)
3. Y.S. Lin, K.J. Ma, C. Hsu, S.W. Feng, Y.C. Cheng, C.C. Liao, C.C. Yang, C.C. Chuo, C.M. Lee, J.I. Chyi, Appl. Phys. Lett. **77**, 2988 (2000)
4. T. Hino, S. Tomiya, T. Miyajima, K. Yanashima, S. Hashimoto, M. Ikeda, Appl. Phys. Lett. **76**, 3421 (2000)
5. Y.H. Cho, G.H. Gainer, A.J. Fischer, J.J. Song, S. Keller, U.K. Mishra, S.P. DenBarrs, Appl. Phys. Lett. **73**, 1370 (1998)
6. P. Riblet, H. Hirayama, A. Kinoshita, A. Hirata, T. Sugano, Y. Aoyagi, Appl. Phys. Lett. **75**, 2241 (1999)
7. S.F. Chichibu, A.C. Abare, M.S. Minsky, S. Keller, S.B. Fleischer, J.E. Bowers, E. Hu, U.K. Mishra, L.A. Coldren, S.P. DenBaars, T. Sota, Appl. Phys. Lett. **73**, 2006 (1998)
8. C.K. Choi, Y.M. Kwon, B.D. Little, G.H. Gainer, J.J. Song, Y.C. Chang, Phys. Rev. B **64**, 245339 (2001)
9. R. Langer, J. Simon, V. Oritz, N.T. Pelekanos, A. Barski, R. André, M. Godlewski, Appl. Phys. Lett. **74**, 3827 (1999)
10. P. Waltereit, O. Brandt, A. Trampert, H.T. Grahn, J. Menniger, M. Ramsteiner, M. Reiche, K.H. Ploog, Nature **406**, 865 (2000)
11. I.H. Ho, G.B. Stringfellow, Appl. Phys. Lett. **69**, 2701 (1996)
12. S. Chichibu, T. Azuhata, T. Soda, S. Nakamura, Appl. Phys. Lett. **69**, 4188 (1996)
13. S. Chichibu, T. Azuhata, T. Sota, S. Nakamura, Appl. Phys. Lett. **70**, 2822 (1997)
14. M.S. Minsky, S.B. Fleischer, A.C. Abare, J.E. Bowers, E.L. Hu, S. Keller, S.P. Denbaars, Appl. Phys. Lett. **72**, 1066 (1998)
15. J. Bai, T. Wang, S. Sakai, J. Appl. Phys. **88**, 4729 (2000)
16. T. Wang, D. Nakagawa, M. Lachab, T. Sugahara, S. Sakai, Appl. Phys. Lett. **74**, 3128 (1999)
17. D. Bimberg, M. Grundmann, N.N. Ledentsov, *Quantum Dot Heterostructures* (Wiley, Chichester, 1999)
18. T.M. Hsu, Y.S. Lan, W.H. Chang, N.T. Yeh, J.I. Chyi, Appl. Phys. Lett. **76**, 691 (2000)
19. W.H. Lee, K.S. Kim, G.M. Yang, C.H. Hong, K.Y. Lim, E.K. Suh, H.J. Lee, H.K. Cho, J.Y. Lee, J. Korean Phys. Soc. **39**, 136 (2001)
20. L.T. Romano, M.D. McCluskey, B.S. Krusor, D.P. Bour, C. Chua, S. Brennan, K.M. Yu, J. Crystal Growth **189/190**, 33 (1998)
21. C.C. Chuo, C.M. Lee, T.E. Nee, J.I. Chyi, Appl. Phys. Lett. **76**, 3902 (2000)
22. Y.S. Lin, K.J. Ma, C. Hsu, Y.Y. Chung, C.W. Liu, S.W. Feng, Y.C. Cheng, M.H. Mao, C.C. Yang, H.W. Chuang, C.T. Kuo, J.S. Tsang, T.E. Weirich, Appl. Phys. Lett. **80**, 2571 (2002)
23. O. Ambacher, H. Angerer, R. Dimitrov, W. Rieger, M. Stutzmann, G. Dollinger, A. Bergmaier, Hydrogen in gallium nitride growth by MOCVD. Phys. Status Solidi A **159**(1), 105–112 (1997)
24. L. Vegard, H. Dale, Untersuchungen über Mischkristalle und Legierungen. Z. Kristallogr. **67**, 148–162 (1928)
25. A. Strecker, U. Salzberger, J. Mayer, Specimen preparation for transmission electron microscopy: reliable method for cross-sections and brittle materials. Prakt. Metallogr. **30**, 482–495 (1993)
26. F. Hofer, P. Warbichler, Elemental mapping using energy filtered imaging, in *Transmission Electron Energy Loss Spectrometry in Materials Science and the EELS ATLAS*, ed. by C.C. Ahn (Wiley-VCH Verlag, Weinheim, 2004), pp. 159–222
27. M.J. Hytch, Analysis of variations in structure from high resolution electron microscope images by combining real space and fourier space information. Microsc. Microanal. Microstruct. **8**, 41–57 (1997)
28. Y.Y. Chung, Y.S. Lin, S.W. Feng, Y.C. Cheng, E.C. Lin, C.C. Yang, K.J. Ma, C. Hsu, H.W. Chuang, C.T. Kuo, J.S. Tsang, Quantum-well-width dependencies of post-growth thermal annealing effects of InGaN/GaN quantum wells. J. Appl. Phys. **93**, 9693–9696 (2003)
29. T.M. Smeeton, M.J. Kappers, J.S. Barnard, M.E. Vickers, C.J. Humphreys, Appl. Phys. Lett. **83**(26), 5419–5421 (2003)